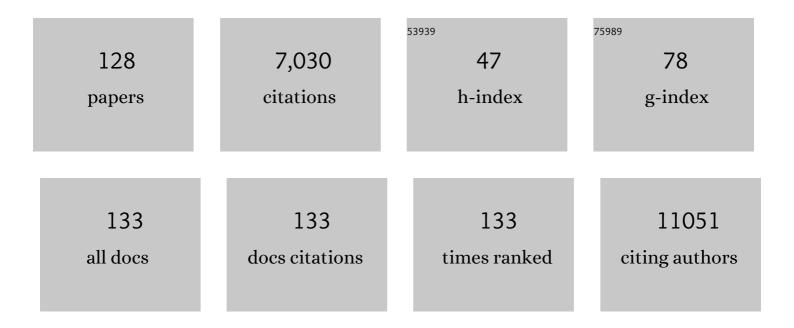
List of Publications by Year in descending order

Source: https://exaly.com/author-pdf/5738071/publications.pdf Version: 2024-02-01



VIIKI SUCILIDA

#	Article	IF	CITATIONS
1	A method for determination of aldosterone concentrations of six adrenal venous serum samples during a single LC/ESI-MS/MS run using a sextet of Girard reagents. Journal of Pharmaceutical and Biomedical Analysis, 2022, 207, 114423.	1.4	7
2	Optogenetic stimulus-triggered acquisition of seizure resistance. Neurobiology of Disease, 2022, 163, 105602.	2.1	12
3	Cancer-derived cholesterol sulfate is a key mediator to prevent tumor infiltration by effector T cells. International Immunology, 2022, 34, 277-289.	1.8	12
4	Tumor-specific interendothelial adhesion mediated by FLRT2 facilitates cancer aggressiveness. Journal of Clinical Investigation, 2022, 132, .	3.9	13
5	Familial Hyperaldosteronism Type 3 with a Rapidly Growing Adrenal Tumor: An In Situ Aldosterone Imaging Study. Current Issues in Molecular Biology, 2022, 44, 128-138.	1.0	6
6	Pharmacological intervention of cholesterol sulfate-mediated T cell exclusion promotes antitumor immunity. Biochemical and Biophysical Research Communications, 2022, 609, 183-188.	1.0	7
7	Coupling of angiogenesis and odontogenesis orchestrates tooth mineralization in mice. Journal of Experimental Medicine, 2022, 219, .	4.2	12
8	Senolysis by glutaminolysis inhibition ameliorates various age-associated disorders. Science, 2021, 371, 265-270.	6.0	222
9	Mutant ASXL1 induces age-related expansion of phenotypic hematopoietic stem cells through activation of Akt/mTOR pathway. Nature Communications, 2021, 12, 1826.	5.8	54
10	Rostro-caudal different energy metabolism leading to differences in degeneration in spinal cord injury. Brain Communications, 2021, 3, fcab058.	1.5	8
11	Staphylococcus cohnii is a potentially biotherapeutic skin commensal alleviating skin inflammation. Cell Reports, 2021, 35, 109052.	2.9	26
12	Mass Spectrometric Enzyme Histochemistry for Choline Acetyltransferase Reveals De Novo Acetylcholine Synthesis in Rodent Brain and Spinal Cord. ACS Chemical Neuroscience, 2021, 12, 2079-2087.	1.7	6
13	What Do We See in Spectra?: Assignment of High-Intensity Peaks of Cutibacterium and Staphylococcus Spectra of MALDI-TOF Mass Spectrometry by Interspecies Comparative Proteogenomics. Microorganisms, 2021, 9, 1243.	1.6	1
14	Possible Therapeutic Strategy Involving the Purine Synthesis Pathway Regulated by ITK in Tongue Squamous Cell Carcinoma. Cancers, 2021, 13, 3333.	1.7	4
15	SLC15A4 mediates M1-prone metabolic shifts in macrophages and guards immune cells from metabolic stress. Proceedings of the National Academy of Sciences of the United States of America, 2021, 118, .	3.3	29
16	A sublethal ATP11A mutation associated with neurological deterioration causes aberrant phosphatidylcholine flipping in plasma membranes. Journal of Clinical Investigation, 2021, 131, .	3.9	25
17	Gut bacteria identified in colorectal cancer patients promote tumourigenesis via butyrate secretion. Nature Communications, 2021, 12, 5674.	5.8	95
18	AKT signaling is associated with epigenetic reprogramming via the upregulation of TET and its cofactor, alpha-ketoglutarate during iPSC generation. Stem Cell Research and Therapy, 2021, 12, 510.	2.4	7

#	Article	IF	CITATIONS
19	Osteoclasts adapt to physioxia perturbation through DNA demethylation. EMBO Reports, 2021, 22, e53035.	2.0	13
20	Structural library and visualization of endogenously oxidized phosphatidylcholines using mass spectrometry-based techniques. Nature Communications, 2021, 12, 6339.	5.8	24
21	B cell-derived GABA elicits IL-10+ macrophages toÂlimit anti-tumour immunity. Nature, 2021, 599, 471-476.	13.7	145
22	In Vivo Hypoglycemic Effects, Potential Mechanisms and LC-MS/MS Analysis of Dendropanax Trifidus Sap Extract. Nutrients, 2021, 13, 4332.	1.7	2
23	Extracellular ATP Limits Homeostatic T Cell Migration Within Lymph Nodes. Frontiers in Immunology, 2021, 12, 786595.	2.2	8
24	Quantitative MALDI-MS/MS assay for serum cortisol through charged derivatization. Journal of Pharmaceutical and Biomedical Analysis, 2020, 178, 112912.	1.4	5
25	Short-chain fatty acids bind to apoptosis-associated speck-like protein to activate inflammasome complex to prevent Salmonella infection. PLoS Biology, 2020, 18, e3000813.	2.6	32
26	Vitamin B1 Supports the Differentiation of T Cells through TGF-Î ² Superfamily Production in Thymic Stromal Cells. IScience, 2020, 23, 101426.	1.9	14
27	C-type lectin Mincle mediates cell death–triggered inflammation in acute kidney injury. Journal of Experimental Medicine, 2020, 217, .	4.2	35
28	Progesterone receptor membrane associated component 1 enhances obesity progression in mice by facilitating lipid accumulation in adipocytes. Communications Biology, 2020, 3, 479.	2.0	23
29	In situ imaging of monoamine localization and dynamics. , 2020, 208, 107478.		4
30	Starvation causes female-to-male sex reversal through lipid metabolism in the teleost fish, medaka (<i>Olyzias latipes</i>). Biology Open, 2020, 9, .	0.6	31
31	IMP dehydrogenase-2 drives aberrant nucleolar activity and promotes tumorigenesis in glioblastoma. Nature Cell Biology, 2019, 21, 1003-1014.	4.6	107
32	<i>Dendropanax morbiferus</i> leaf extract facilitates oligodendrocyte development. Royal Society Open Science, 2019, 6, 190266.	1.1	5
33	Detection of a High-Turnover Serotonin Circuit in the Mouse Brain Using Mass Spectrometry Imaging. IScience, 2019, 20, 359-372.	1.9	33
34	A defined commensal consortium elicits CD8 T cells and anti-cancer immunity. Nature, 2019, 565, 600-605.	13.7	741
35	Tandem Mass Spectrometry Imaging Reveals Distinct Accumulation Patterns of Steroid Structural Isomers in Human Adrenal Glands. Analytical Chemistry, 2019, 91, 8918-8925.	3.2	48
36	Mechanical allodynia induced by optogenetic sensory nerve excitation activates dopamine signaling and metabolism in medial nucleus accumbens. Neurochemistry International, 2019, 129, 104494.	1.9	9

#	Article	IF	CITATIONS
37	A thin layer of sucrose octasulfate protects the oesophageal mucosal epithelium in reflux oesophagitis. Scientific Reports, 2019, 9, 3559.	1.6	2
38	Autophagy regulates lipid metabolism through selective turnover of NCoR1. Nature Communications, 2019, 10, 1567.	5.8	143
39	Increased Cytotoxicity of Herpes Simplex Virus Thymidine Kinase Expression in Human Induced Pluripotent Stem Cells. International Journal of Molecular Sciences, 2019, 20, 810.	1.8	20
40	Immunohistochemistry for aldosterone synthase CYP11B2 and matrix-assisted laser desorption ionization imaging mass spectrometry for in-situ aldosterone detection. Current Opinion in Nephrology and Hypertension, 2019, 28, 105-112.	1.0	8
41	Gold-nanofève surface-enhanced Raman spectroscopy visualizes hypotaurine as a robust anti-oxidant consumed in cancer survival. Nature Communications, 2018, 9, 1561.	5.8	74
42	Extracellular N-acetylaspartylglutamate released in the nucleus accumbens modulates the pain sensation: Analysis using a microdialysis/mass spectrometry integrated system. Molecular Pain, 2018, 14, 174480691875493.	1.0	12
43	Utilizing mass spectrometry imaging to map the thyroid hormones triiodothyronine and thyroxine in Xenopus tropicalis tadpoles. Analytical and Bioanalytical Chemistry, 2018, 410, 1333-1340.	1.9	11
44	PKM1 Confers Metabolic Advantages and Promotes Cell-Autonomous Tumor Cell Growth. Cancer Cell, 2018, 33, 355-367.e7.	7.7	121
45	Aldosterone and 18-Oxocortisol Coaccumulation in Aldosterone-Producing Lesions. Hypertension, 2018, 72, 1345-1354.	1.3	44
46	Optogenetic astrocyte activation evokes BOLD fMRI response with oxygen consumption without neuronal activity modulation. Glia, 2018, 66, 2013-2023.	2.5	72
47	Cholesterol sulfate is a DOCK2 inhibitor that mediates tissue-specific immune evasion in the eye. Science Signaling, 2018, 11, .	1.6	29
48	Sodium–glucose cotransporter 2 inhibition normalizes glucose metabolism and suppresses oxidative stress in the kidneys of diabetic mice. Kidney International, 2018, 94, 912-925.	2.6	123
49	A method for determination of aldosterone in adrenal tributary venous serum by derivatization using Girard P reagent isotopologues followed by LC/ESI-MS/MS. Journal of Chromatography B: Analytical Technologies in the Biomedical and Life Sciences, 2018, 1092, 106-113.	1.2	18
50	Utilizing mass spectrometry imaging to map the thyroid hormones triiodothyronine and thyroxine in Xenopus tropicalis tadpoles. , 2018, 410, 1333.		1
51	Rewiring of embryonic glucose metabolism via suppression of PFK-1 and aldolase during mouse chorioallantoic branching. Development (Cambridge), 2017, 144, 63-73.	1.2	70
52	Placental labyrinth formation in mice requires endothelial FLRT2–UNC5B signaling. Development (Cambridge), 2017, 144, 2392-2401.	1.2	21
53	Decreased 16:0/20:4-phosphatidylinositol level in the post-mortem prefrontal cortex of elderly patients with schizophrenia. Scientific Reports, 2017, 7, 45050.	1.6	19
54	Metabolic shift induced by systemic activation of T cells in PD-1-deficient mice perturbs brain monoamines and emotional behavior. Nature Immunology, 2017, 18, 1342-1352.	7.0	83

#	Article	IF	CITATIONS
55	Arl8b is required for lysosomal degradation of maternal proteins in the visceral yolk sac endoderm of mouse embryos. Journal of Cell Science, 2017, 130, 3568-3577.	1.2	23
56	Hydrophilic Metabolite Analysis. Journal of the Mass Spectrometry Society of Japan, 2017, 65, 195-198.	0.0	1
57	Rewiring of embryonic glucose metabolism via suppression of PFK-1 and aldolase during mouse chorioallantoic branching. Journal of Cell Science, 2017, 130, e1.1-e1.1.	1.2	0
58	Cystathionine Î ² -synthase and PGRMC1 as CO sensors. Free Radical Biology and Medicine, 2016, 99, 333-344.	1.3	23
59	Visualization of Localized Cellular Signalling Mediators in Tissues by Imaging Mass Spectrometry. , 2016, , 147-160.		0
60	Visualization of in vivo metabolic flows reveals accelerated utilization of glucose and lactate in penumbra of ischemic heart. Scientific Reports, 2016, 6, 32361.	1.6	47
61	HIF-1α-PDK1 axis-induced active glycolysis plays an essential role in macrophage migratory capacity. Nature Communications, 2016, 7, 11635.	5.8	233
62	Haem-dependent dimerization of PGRMC1/Sigma-2 receptor facilitates cancer proliferation and chemoresistance. Nature Communications, 2016, 7, 11030.	5.8	153
63	Fibroblastic reticular cell-derived lysophosphatidic acid regulates confined intranodal T-cell motility. ELife, 2016, 5, e10561.	2.8	45
64	Development of an Imaging Mass Spectrometry Technique for Visualizing Localized Cellular Signaling Mediators in Tissues. Mass Spectrometry, 2015, 4, A0040-A0040.	0.2	13
65	Hypoperfusion of the Adventitial Vasa Vasorum Develops an Abdominal Aortic Aneurysm. PLoS ONE, 2015, 10, e0134386.	1.1	70
66	Mode of Bioenergetic Metabolism during B Cell Differentiation in the Intestine Determines the Distinct Requirement for Vitamin B1. Cell Reports, 2015, 13, 122-131.	2.9	96
67	Therapeutic Hypothermia Achieves Neuroprotection <i>via</i> a Decrease in Acetylcholine with a Concurrent Increase in Carnitine in the Neonatal Hypoxia-Ischemia. Journal of Cerebral Blood Flow and Metabolism, 2015, 35, 794-805.	2.4	31
68	Finding of thiosulfate pathway for synthesis of organic sulfur compounds in Saccharomyces cerevisiae and improvement of ethanol production. Journal of Bioscience and Bioengineering, 2015, 120, 666-669.	1.1	19
69	Direct profiling of the phospholipid composition of adult Caenorhabditis elegans using whole-body imaging mass spectrometry. Analytical and Bioanalytical Chemistry, 2015, 407, 7589-7602.	1.9	9
70	Effective Sample Preparations in Imaging Mass Spectrometry. Mass Spectrometry, 2014, 3, S0029-S0029.	0.2	33
71	Nonâ€neuronal acetylcholine as an endogenous regulator of proliferation and differentiation of Lgr5â€positive stem cells in mice. FEBS Journal, 2014, 281, 4672-4690.	2.2	59
72	Microscopic imaging mass spectrometry assisted by onâ€tissue chemical derivatization for visualizing multiple amino acids in human colon cancer xenografts. Proteomics, 2014, 14, 810-819.	1.3	65

#	Article	IF	CITATIONS
73	Characterization of the 17 strains of regulatory T cell-inducing human-derived Clostridia. Gut Microbes, 2014, 5, 333-339.	4.3	182
74	Visualization and quantification of cerebral metabolic fluxes of glucose in awake mice. Proteomics, 2014, 14, 829-838.	1.3	61
75	Arundic acid (ONO-2506) inhibits secondary injury and improves motor function in rats with spinal cord injury. Journal of the Neurological Sciences, 2014, 337, 186-192.	0.3	15
76	Endogenous Prostaglandin D ₂ and Its Metabolites Protect the Heart Against Ischemia–Reperfusion Injury by Activating Nrf2. Hypertension, 2014, 63, 80-87.	1.3	79
77	Evaluation of the effect of tranilast on rats with spinal cord injury. Journal of the Neurological Sciences, 2014, 346, 209-215.	0.3	10
78	The Histidine Transporter SLC15A4 Coordinates mTOR-Dependent Inflammatory Responses and Pathogenic Antibody Production. Immunity, 2014, 41, 375-388.	6.6	121
79	DHA-PC and PSD-95 decrease after loss of synaptophysin and before neuronal loss in patients with Alzheimer's disease. Scientific Reports, 2014, 4, 7130.	1.6	135
80	Sulfatide accumulation in the dystrophic terminals of gracile axonal dystrophy mice: lipid analysis using matrix-assisted laser desorption/ionization imaging mass spectrometry. Medical Molecular Morphology, 2013, 46, 160-165.	0.4	10
81	Energy Management by Enhanced Glycolysis in G1-phase in Human Colon Cancer Cells <i>In Vitro</i> and <i>In Vivo</i> . Molecular Cancer Research, 2013, 11, 973-985.	1.5	58
82	Constitutive Lymphocyte Transmigration across the Basal Lamina of High Endothelial Venules Is Regulated by the Autotaxin/Lysophosphatidic Acid Axis. Journal of Immunology, 2013, 190, 2036-2048.	0.4	95
83	Axonal Gradient of Arachidonic Acid-containing Phosphatidylcholine and Its Dependence on Actin Dynamics. Journal of Biological Chemistry, 2012, 287, 5290-5300.	1.6	41
84	Spatiotemporal alteration of phospholipids and prostaglandins in a rat model of spinal cord injury. Analytical and Bioanalytical Chemistry, 2012, 403, 1873-1884.	1.9	39
85	Visualization of acetylcholine distribution in central nervous system tissue sections by tandem imaging mass spectrometry. Analytical and Bioanalytical Chemistry, 2012, 403, 1851-1861.	1.9	69
86	Method for Simultaneous Imaging of Endogenous Low Molecular Weight Metabolites in Mouse Brain Using TiO ₂ Nanoparticles in Nanoparticle-Assisted Laser Desorption/Ionization-Imaging Mass Spectrometry. Analytical Chemistry, 2011, 83, 7283-7289.	3.2	96
87	Hydroxylated and non-hydroxylated sulfatide are distinctly distributed in the human cerebral cortex. Neuroscience, 2011, 193, 44-53.	1.1	55
88	Using Imaging Mass Spectrometry to Accurately Diagnose Fabry's Disease. Circulation Journal, 2011, 75, 221-223.	0.7	15
89	Abnormal phospholipids distribution in the prefrontal cortex from a patient with schizophrenia revealed by matrix-assisted laser desorption/ionization imaging mass spectrometry. Analytical and Bioanalytical Chemistry, 2011, 400, 1933-1943.	1.9	63
90	Visualization of phosphatidylcholine, lysophosphatidylcholine and sphingomyelin in mouse tongue body by matrix-assisted laser desorption/ionization imaging mass spectrometry. Analytical and Bioanalytical Chemistry, 2011, 400, 1913-1921.	1.9	32

#	Article	IF	CITATIONS
91	Investigation by Imaging Mass Spectrometry of Biomarker Candidates for Aging in the Hair Cortex. PLoS ONE, 2011, 6, e26721.	1.1	20
92	Neuroaxonal Dystrophy in Calcium-Independent Phospholipase A ₂ β Deficiency Results from Insufficient Remodeling and Degeneration of Mitochondrial and Presynaptic Membranes. Journal of Neuroscience, 2011, 31, 11411-11420.	1.7	105
93	Visualization of Spatiotemporal Energy Dynamics of Hippocampal Neurons by Mass Spectrometry during a Kainate-Induced Seizure. PLoS ONE, 2011, 6, e17952.	1.1	72
94	Ionic Matrix for Enhanced MALDI Imaging Mass Spectrometry for Identification of Phospholipids in Mouse Liver and Cerebellum Tissue Sections. Analytical Chemistry, 2010, 82, 8800-8806.	3.2	57
95	Detection of characteristic distributions of phospholipid head groups and fatty acids on neurite surface by time-of-flight secondary ion mass spectrometry. Medical Molecular Morphology, 2010, 43, 158-164.	0.4	37
96	Developments and applications of mass microscopy. Medical Molecular Morphology, 2010, 43, 1-5.	0.4	26
97	Imaging Mass Spectrometry for Visualization of Drug and Endogenous Metabolite Distribution: Toward In Situ Pharmacometabolomes. Journal of NeuroImmune Pharmacology, 2010, 5, 31-43.	2.1	132
98	Imaging of lipids in cultured mammalian neurons by matrix assisted laser/desorption ionization and secondary ion mass spectrometry. Surface and Interface Analysis, 2010, 42, 1606-1611.	0.8	22
99	Imaging mass spectrometry revealed the production of lyso-phosphatidylcholine in the injured ischemic rat brain. Neuroscience, 2010, 168, 219-225.	1.1	121
100	Matrix-Assisted Laser Desorption/Ionization and Nanoparticle-Based Imaging Mass Spectrometry for Small Metabolites: A Practical Protocol. Methods in Molecular Biology, 2010, 656, 173-195.	0.4	9
101	Imaging of Cultured Cells by Mass Spectrometry. , 2010, , 159-168.		2
102	Imaging and Molecular Identification of Biomolecules on Tissue Sections with AXIMA-QIT: Shimadzu Corporation. , 2010, , 209-219.		1
103	MALDI Imaging with Ion-Mobility MS: Waters Corporation. , 2010, , 221-231.		1
104	Guide to Planning the Sample Preparation Step. , 2010, , 11-30.		4
105	Preparing Biological Tissue Sections for Imaging Mass Spectrometry. , 2010, , 41-54.		4
106	Matrix Choice. , 2010, , 55-69.		6
107	Methods of Matrix Application. , 2010, , 71-85.		9
108	Ion Image Reconstruction Using BioMap Software. , 2010, , 113-126.		5

#	Article	IF	CITATIONS
109	Layer-specific sulfatide localization in rat hippocampus middle molecular layer is revealed by nanoparticle-assisted laser desorption/ionization imaging mass spectrometry. Medical Molecular Morphology, 2009, 42, 16-23.	0.4	54
110	Medical molecular morphology with imaging mass spectrometry. Medical Molecular Morphology, 2009, 42, 133-137.	0.4	12
111	Selective imaging of positively charged polar and nonpolar lipids by optimizing matrix solution composition. Rapid Communications in Mass Spectrometry, 2009, 23, 3269-3278.	0.7	63
112	Visualization of Volatile Substances in Different Organelles with an Atmospheric-Pressure Mass Microscope. Analytical Chemistry, 2009, 81, 9153-9157.	3.2	127
113	Recombinant Mammalian Tubulin Polyglutamylase TTLL7 Performs both Initiation and Elongation of Polyglutamylation on β-Tubulin through a Random Sequential Pathway. Biochemistry, 2009, 48, 1084-1093.	1.2	39
114	Visualization of the cell-selective distribution of PUFA-containing phosphatidylcholines in mouse brain by imaging mass spectrometry. Journal of Lipid Research, 2009, 50, 1776-1788.	2.0	180
115	Magnetic Nanoparticle-Based Mass Spectrometry for the Detection of Biomolecules in Cultured Cells. Journal of Nanoscience and Nanotechnology, 2009, 9, 169-176.	0.9	26
116	High-sensitivity analysis of glycosphingolipids by matrix-assisted laser desorption/ionization quadrupole ion trap time-of-flight imaging mass spectrometry on transfer membranes. Journal of Chromatography B: Analytical Technologies in the Biomedical and Life Sciences, 2008, 870, 74-83.	1.2	59
117	<i>In situ</i> proteomics with imaging mass spectrometry and principal component analysis in the <i>Scrapper</i> â€knockout mouse brain. Proteomics, 2008, 8, 3692-3701.	1.3	71
118	Matrixâ€assisted laser desorption/ionization quadrupole ion trap timeâ€ofâ€flight (MALDIâ€QITâ€TOF)â€based imaging mass spectrometry reveals a layered distribution of phospholipid molecular species in the mouse retina. Rapid Communications in Mass Spectrometry, 2008, 22, 3415-3426.	0.7	119
119	Protein denaturation improves enzymatic digestion efficiency for direct tissue analysis using mass spectrometry. Applied Surface Science, 2008, 255, 1555-1559.	3.1	14
120	Nanoparticle-Assisted Laser Desorption/Ionization Based Mass Imaging with Cellular Resolution. Analytical Chemistry, 2008, 80, 4761-4766.	3.2	164
121	Mass Imaging and Identification of Biomolecules with MALDI-QIT-TOF-Based System. Analytical Chemistry, 2008, 80, 878-885.	3.2	155
122	Imaging Mass Spectrometry Technology and Application on Ganglioside Study; Visualization of Age-Dependent Accumulation of C20-Ganglioside Molecular Species in the Mouse Hippocampus. PLoS ONE, 2008, 3, e3232.	1.1	139
123	Spectrum Normalization Method Using an External Standard in Mass Spectrometric Imaging. Journal of the Mass Spectrometry Society of Japan, 2008, 56, 77-81.	0.0	15
124	MALDI-based imaging mass spectrometry revealed abnormal distribution of phospholipids in colon cancer liver metastasis. Journal of Chromatography B: Analytical Technologies in the Biomedical and Life Sciences, 2007, 855, 98-103.	1.2	168
125	Direct Analysis of Cultured Cells with Matrix-Assisted Laser Desorption/Ionization on Conductive Transparent Film. Journal of the Mass Spectrometry Society of Japan, 2007, 55, 25-31.	0.0	8
126	Two-Step Matrix Application Technique To Improve Ionization Efficiency for Matrix-Assisted Laser Desorption/Ionization in Imaging Mass Spectrometry. Analytical Chemistry, 2006, 78, 8227-8235.	3.2	110

#	Article	IF	CITATIONS
127	2P545 Imaging and direct structural analysis of biomolecules on the mammalian tissue surface using tandem mass spectrometry(52. Bio-imaging,Poster Session,Abstract,Meeting Program of EABS & amp; BSJ) 1	՟j ETQq b. b0.78	343014 rgBT /C
	Thin Sectioning Improves the Peab Intensity and Signal-to-Noise Ratio in Direct Tissue Mass		

128 Thin Sectioning Improves the Peak Intensity and Signal-to-Noise Ratio in Direct Tissue Mass Spectrometry. Journal of the Mass Spectrometry Society of Japan, 2006, 54, 45-48.

0.0 79